

Rashba Spin Orbit Interaction and Birefringent Electron Optics in Graphene

Mahmoud M. Asmar* and Sergio E. Ulloa†

*Department of Physics and Astronomy and Nanoscale and Quantum Phenomena Institute,
Ohio University, Athens, Ohio 45701-2979, USA*

Electron optics exploits the analogies between rays in geometrical optics and electron trajectories, leading to interesting insights and potential applications. Graphene, with its two-dimensionality and photon-like behavior of its charge carriers, is the perfect candidate for the exploitation of electron optics. We show that a circular gate- or doping-controlled region in the presence of Rashba spin-orbit interaction in graphene may indeed behave as a Veselago electronic lens but with two different indices of refraction. We demonstrate that this birefringence results in complex caustics patterns for a circular gate, selective focusing of different spins, and the possible direct measurement of the Rashba coupling strength in scanning probe experiments.

PACS numbers: 71.70.Ej, 75.76.+j, 72.10.Fk, 42.25.Lc

The analogies between geometrical optics and electron trajectories have resulted in a number of interesting proposals for device applications [1], where interfaces play a similar role to that played by transparent interfaces in physical optics. This leads to the manipulation and control of electron trajectories, where the major factor determining the electron dynamics is the change in group velocity through these interfaces, mimicking refringent physical optics and lenses. Such change in group velocity is typically achieved by local gating, which modulates carrier densities and fixes the corresponding index of refraction.

Optical birefringence in materials results from crystal anisotropies which are manifested as different group velocities for different polarizations of the propagating light in the material. In this paper, we show that an equivalent phenomenon to optical birefringence in electron optics is feasible in two dimensional graphene, which in essence reflects the intrinsic crystal structure even at large electronic wavelengths. The effect requires the presence of Rashba spin-orbit interaction, where the different group velocities depend on the chirality of the electronic states, mimicking the light polarization dependence of the group velocities in optical birefringent materials.

The low energy dispersion of electrons in graphene is centered near two inequivalent points in the Brillouin zone, the K and K' or Dirac points [2–4]. The “massless” nature of electrons results in novel phenomena such as the Klein paradox [3, 5, 6], which leads to full transparency of a sharp gated interface for normal incident electrons, and a high probability of transmission for incoming electrons with finite angles. The linear dispersion of electrons is also evocative of photons, prompting a number of proposals and experiments to probe optical analogs with charge carriers [7], aided in great measure by the high electron mobility in this unique material. In fact, the transparency of barriers and ability to gate regions of the system to change the sign of carriers can lead to the use of graphene gate-controlled interfaces as electronic lenses that follow Snell’s law with negative index

of refraction and allow the implementation of electronic analogues of Veselago optics [8–10].

The study of spin transport properties of suspended and deposited graphene is rapidly becoming an important area of research. Experiments have achieved spin polarized injection of electrons and measure spin valve effects [11–13], spin polarized currents with long coherence lengths in suspended graphene [14], and shorter coherence lengths for deposited samples or samples containing impurities that enhance spin orbit effects [15, 16], such as hydrogen or gold [17, 18]. An important ingredient determining the carrier spin dynamics in this and other materials is the spin orbit interaction (SOI). The *intrinsic* SOI respects all the lattice symmetries in graphene and results in a small energy gap at the Dirac points [19]. The *extrinsic* or Rashba SOI results from the lack of inversion symmetry due to perpendicular electric fields, substrate effects, chemical doping, or curvature of graphene corrugations [20, 21]. In this paper we focus on the effects of the Rashba SOI in the spin dynamics of carriers away from the neutrality point as the spin-orbit interaction can be controlled by external factors [22].

To study these effects, we consider a graphene sheet with a circular gate potential (or corresponding doping/intercalation profile) covering an area of radius R , where the electric field (or doping) reverses the carrier character from electron to hole and also generates a Rashba SOI of strength λ_R , as shown in Figure 1a. Electron scattering from such gated regions has been shown to result in pronounced wave function intensity maxima due the constructive interference between different partial wave components [8]. These patterns are similar to the optical caustics which develop by light refraction through a shaped medium, and belong to a class of cusps in catastrophe theory [23]. We should comment that recent experiments have demonstrated gate tunability, which makes the study of electron optics on graphene viable and controllable [6, 24, 25]. Moreover, imaging of the patterns resulting from the electron flow through these nanoscale structures can be achieved through STM

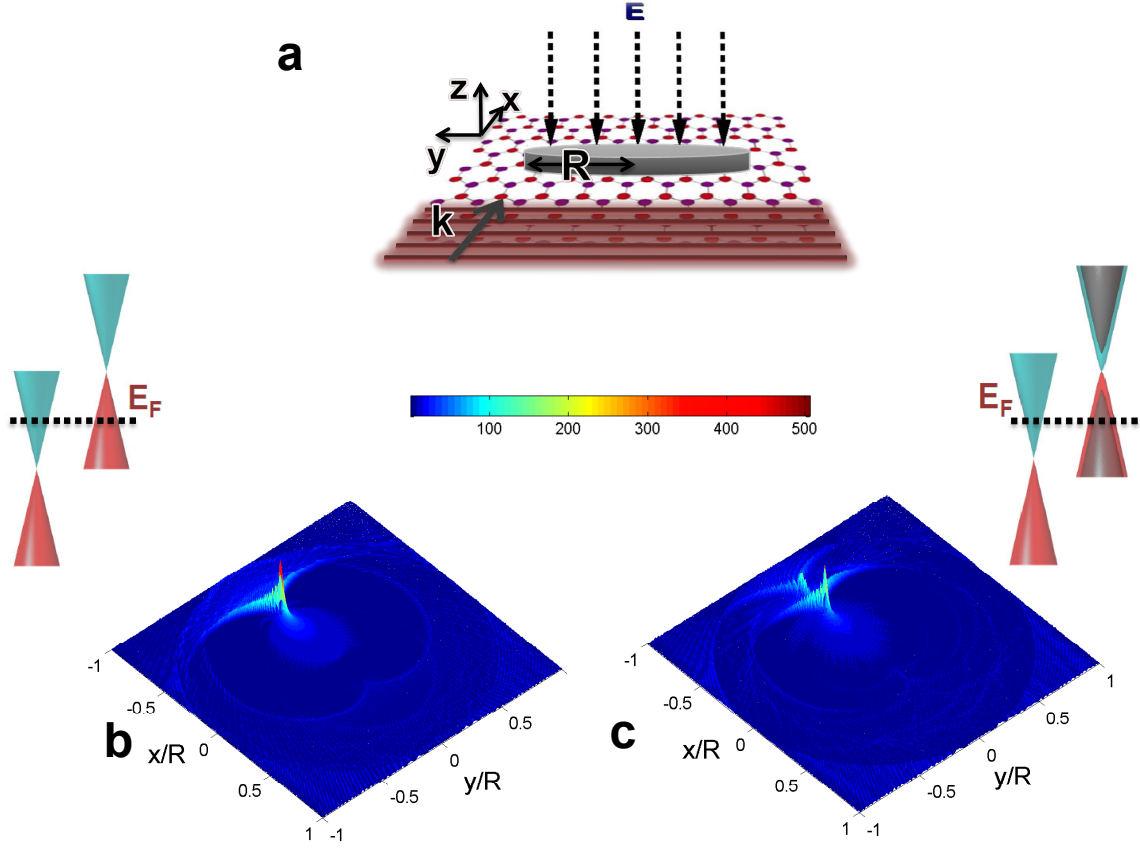


FIG. 1. (Color online) **a**) Electron flux in graphene coming along the x -direction onto a circular gate potential covering an area of radius R ; the normal electric field reverses the carrier character from electron to hole and also generates a Rashba spin-orbit field. **b**) Three dimensional map of $|\psi|^2$ near and inside gated region centered at $(x, y) = (0, 0)$ (normalized to incident flux). The electronic patterns produced inside the gated region are analogous to those produced by the refraction of light in a circular medium with refractive index $n = -1$ (Veselago lens). The electronic index of refraction is determined by the ratio of wave numbers in and out of the gated obstacle: both regions are characterized by a linear electronic dispersion (upper left inset), and in this case, $kR = 300$ (electron) and $k'R = 300$ (hole). High intensity maxima correspond to caustics with $p = 1$ ($x < 0$) and $p = 2$ ($x > 0$), where $p - 1$ is the number of internal reflections. x and y coordinates in units of the radius R . **c**) In the presence of Rashba spin orbit interaction the electronic dispersion in the gated region is modified, so that scattering particles have access to two different wave numbers (upper right inset). Scattering produces electronic patterns as shown in the three dimensional map $|\psi|^2$, with $kR = 300$, $VR/\hbar v_F = 600$, $\lambda_R R/\hbar v_F = 100$, for \uparrow -spin incoming flux. The $p = 1$ and $p = 2$ caustics and cusps are doubled, associated with states of different chirality in graphene. The pattern can be described by the refraction from a medium with two (negative) indices, n_{\pm} . Here, the degree of birefringence is $\Delta n = n_- - n_+ = 0.71$. The dual pattern persists even for spin-unpolarized incidence.

[26, 27] or other scanning probe techniques [28, 29].

The Hamiltonian of the system has the form $H = H_o + H_V + H_R$, where $H_o/\hbar v_F = \sigma_x k_x + \sigma_y k_y$ describes free electrons in graphene with momentum $\vec{k} = (k_x, k_y)$ away from the K point. $H_V = V\vartheta(R - r)$ represents the gated or doped region of strength V and $H_R = \lambda_R(\sigma_x s_y - s_x \sigma_y)\vartheta(R - r)$ is the Rashba SOI in this circular region for \vec{k} near the K point [4, 19], where $\{\sigma_{\mu}\}$ and $\{s_{\mu}\}$ are Pauli matrices representing the electron pseudospin (A, B) and spin (\uparrow, \downarrow), respectively, λ_R is the strength of the Rashba interaction, and ϑ is the Heaviside function determining the radius R of the region. The Hamiltonian is parameterized in terms of $\hbar v_F$, where $v_F = 10^6 \text{ m/s}$ is the carrier Fermi velocity [2, 3]. We are interested

in Rashba regions with $R \gg a$, where a is the lattice constant of graphene, in order to adopt the continuum description of graphene.

The cylindrical symmetry of the system allows one to write the eigenfunctions in terms of four linear differential equations coupling the different spinor components, $\psi_j = (\psi_{A\uparrow}, \psi_{B\uparrow}, \psi_{A\downarrow}, \psi_{B\downarrow})^T$. The symmetries result in the conservation of the z -component of the total angular momentum in the system, $[J_z, H] = 0$, where $J_z = L_z + \hbar s_z/2 + \hbar \sigma_z/2$, and $L_z = -i\hbar \partial_{\theta}$ is the orbital angular momentum; as such, the eigenstates describing the system can be labeled according to their total angular momentum, j , with $J_z \psi_j = j\hbar \psi_j$ (see Supplemental Material).

The scattering of an incident flux of electrons on the gated obstacle is studied through a spin-dependent generalization of the partial wave component method [30]. This utilizes the analytical solutions for the spinors together with their asymptotic expansions and boundary conditions in order to obtain the scattering amplitudes. The latter allow the direct evaluation of wave functions inside and outside the Rashba region, depending on the incident energy, momentum and spin content of the incident flux, as well as system parameters (see Supplemental Material). The momentum outside the scattering region is given by $k = E/\hbar v_F$, while the momentum inside takes *two different values*, $k_{\pm} = \sqrt{(E - V)^2 \pm 2\lambda_R(E - V)}/\hbar v_F$, for the given energy E , due to the presence of the Rashba SOI (see Figure 1).

Formation of caustics has been described in the absence of SOI [10], resulting in beautiful scattering patterns. The caustics and cusps can be understood in terms of geometrical optics, and characterized by a negative index of refraction $n = -|E - V|/|E| = -k'/k$, where k' is the wave number inside the gated region [8] (Veselago lensing [9]). For an incident electron flux along the x -direction, the position of the cusps produced inside a circular gated region can be shown to be given by $x_{cusp} = (-1)^p/(|n| - 1 + 2p)$, for $p - 1$ internal reflections of the ray inside the region [10] (see Figure 1b).

In contrast, in a system with Rashba SOI the two wave numbers for a given energy allow for two refraction indices, associated with the two chiral solutions of the Dirac equation, $n_{\pm} = -k_{\pm}/k$. Correspondingly, the optical analogue results in two different cusp locations (see Fig. 1c) given by

$$x_{cusp}^{\pm} = \frac{(-1)^p}{|n_{\pm}| - 1 + 2p}. \quad (1)$$

As we will see below, this simple description is borne out by the full quantum calculation of the scattering patterns. We should emphasize that despite the optical analogy, birefringence here has a clear quantum mechanical origin, as the group velocity and built in phases of the different chiral states are different due to the presence of the Rashba interaction.

The presence of the Rashba interaction causes the spin of the incoming electron to precess as it travels along the scattering region; this spin precession is seen as oscillations in the amplitudes of the spin components of the wave function (Rashba oscillations), where a clear spatial frequency can be identified for different λ_R values: shorter precession wavelength for larger λ_R . For small Rashba coupling, the wavelength of these oscillations is comparable to the size of the gated region, leading to the presence of different spins over large areas of the scattering disk. Figure 2a,b shows the wave functions inside and outside the scattering region for spin up and down components for $\lambda_R R/\hbar v_F = 3$; take no-

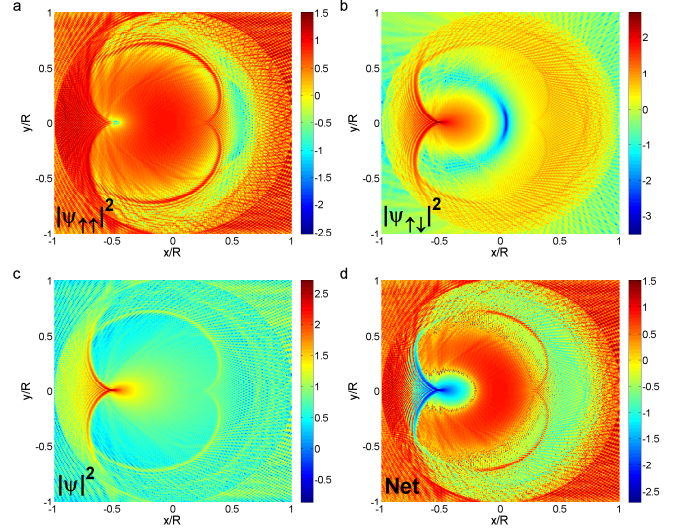


FIG. 2. (Color online) Probability density patterns (scale bars show log of amplitudes, normalized to incident flux) resulting from the scattering of *incoming* \uparrow -spin electron wave along the x -direction with $kR = 300$, in the presence of a gate potential $VR/\hbar v_F = 600$, and Rashba coupling $\lambda_R R/\hbar v_F = 3$. This arrangement leads to a system with a small degree of birefringence $\Delta n = n_- - n_+ = 0.02$. **a)** The spin-preserving component $|\psi_{\uparrow\uparrow}|^2$ and **b)** spin-flip component $|\psi_{\uparrow\downarrow}|^2$ display Rashba oscillations with a wavelength covering a large region of the scattering target, due to the small λ_R . **c)** Total wave function $|\psi|^2 = |\psi_{\uparrow\uparrow}|^2 + |\psi_{\uparrow\downarrow}|^2$, displays caustics and cusps that remain almost unchanged from the case in which the Rashba interaction is absent. **d)** Net spin $\eta \sim |\psi_{\uparrow\uparrow}|^2 - |\psi_{\uparrow\downarrow}|^2$ quantifies the predominance of a given spin in different regions of the system. The large wavelength of Rashba oscillations leads to a cusp at $x \approx -0.5$ with a net \downarrow -spin (blue) while the annular region near $x \approx 0$ has a net \uparrow -spin (red).

tice these are results for *spin-up incidence*. Notice that both spin components display caustics inside the scattering region. Moreover, one observes that the wave function around the caustics has a net spin content, as shown by $\eta = \text{sgn}(\Delta)|\log_{10}(|\Delta|)|$, where $\Delta = |\psi_{\uparrow\uparrow}|^2 - |\psi_{\uparrow\downarrow}|^2$, in Figure 2d. For this set of parameters, the $p = 1$ caustic ($x < 0$) is predominantly spin-down, while the $p = 2$ caustic ($x > 0$) is predominantly spin-up. The total wave function, $|\psi|^2 = |\psi_{\uparrow\uparrow}|^2 + |\psi_{\uparrow\downarrow}|^2$ shows no major changes due to the Rashba SOI, since λ_R is small and the two different wave numbers are nearly equal, $k_- - k_+ \approx 2\lambda_R/\hbar v_F$; see Figure 2c. Correspondingly, the two indices are also very similar, $n_- - n_+ = 0.02$, and the pattern of caustics and cusps is essentially unchanged from the $\lambda_R = 0$ case.

For larger values of the Rashba interaction the oscillations become even sharper, with shorter wavelength, and

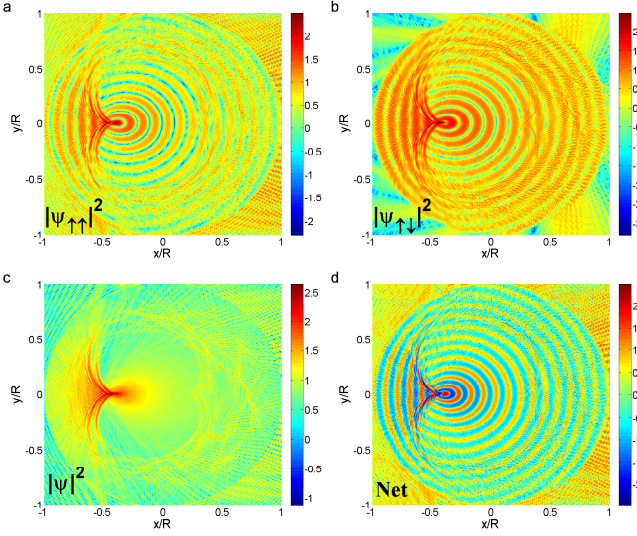


FIG. 3. (Color online) Wave function maps (scale bar show log of amplitudes; normalization to incident flux) similar to those in Figure 2 but for larger λ_R . Here, $kR = 250$, $VR/\hbar v_F = 600$ and $\lambda_R R/\hbar v_F = 30$. This arrangement leads to a system with a degree of birefringence $\Delta n = n_- - n_+ = 0.24$. The different energy of the incoming wave leads to modified positions of caustics and cusps. **a)** $|\psi_{\uparrow\uparrow}|^2$ and **b)** $|\psi_{\uparrow\downarrow}|^2$ show clearer and sharper Rashba oscillations with shorter wavelength. Notice that the number of oscillations inside the gated region is approximately $\lambda_R R/2\hbar v_F = 15$ for both spins, as shown by the rings around the main cusp. **c)** The total wave function, $|\psi|^2$, displays clear duplicate sets of caustics and cusps manifesting the birefringent character of the scattering, due to the large Rashba interaction and associated different group velocities. **d)** The net spin η , shows variation of the two spin components along the the different cusps and caustics.

their number inside the gated region is approximately $\lambda_R R/2\hbar v_F$ for both spins. The larger value of λ_R leads to two very different wave numbers inside the scattering region, k_{\pm} , different group velocities for the charge carriers, and different indices n_{\pm} . In the case of $\lambda_R R/\hbar v_F = 30$, Figure 3, we notice a clear doubling of the cusps, especially evident in panel c for the total wave function. Moreover, the cusp positions are in agreement with the anticipated values shown by Eq. 1, as one can easily verify.

Let us comment on the system conditions for the observation of these effects. We have first assumed a semiclassical limit, with $kR \gg 1$ and $k_{\pm}R \gg 1$; second, we have assumed the absence of intervalley scattering (K to K'), which requires that the characteristic length of potential change must be much larger than the lattice constant. These two rather sensible requirements introduce constraints on the values of the Fermi energy of the incoming electron flux, the gate voltage, and the size of the gated region. Recent experiments have reported values of the Rashba interaction in the range 10-100 meV for graphene samples grown on Ni and inter-

calated with Au atoms [21]. This coupling is 2-3 orders larger than the spatially random spin orbit generated by intrinsic ripples in graphene [20]. Assuming possible values of these parameters in experiments as $E = 80 \text{ meV}$, corresponding to carrier concentration $n_c \simeq 0.5 \times 10^{12} \text{ cm}^{-2}$, $V = 200 \text{ meV}$, and $\lambda_R = 10 \text{ meV}$, would require $R \geq 1000 \text{ nm}$ and lead to $n_- - n_+ \geq 0.24$, allowing the observation of the patterns shown in Figure 3c, and its clear detection in scanning probe experiments, as $|x_{cusp}^+ - x_{cusp}^-| \geq 42 \text{ nm}$. We should also notice that although we have used spin-polarized injection in our calculations, to expose the spin character of the caustic pattern, this is *not* a necessary ingredient to observe the birefringence. Unpolarized electron injection will obviously erase the net spin structures we have discussed. However, the appearance of duplicate caustics and cusps would persist and result in an *identical* spatial structure of the total wave function to the ones shown above. Similarly, K - K' coupling would preserve the duplicate caustic pattern, although with decreased contrast, as the enhanced backscattering would reduce the overall transparency of the region.

In conclusion, we studied the effects of Rashba SOI on the scattering of electrons in graphene. For spin polarized injection, we find a spatial modulation of the carrier spin, with characteristics that depend on the strength of the Rashba interaction and may be important in the implementation of spin based devices in graphene systems. More important, we find the selective formation of spinful cusps and caustics in the region containing large Rashba SOI, opening the possibility of spin beam filters and splitters. Moreover, the manifestation of electronic birefringence at relatively large but experimentally achievable values of the Rashba SOI [21], is the doubling of caustics and cups produced by these refringent Veselago lenses; the spacing between the two different chiral cusps is proportional to the strength of the Rashba interaction in the system. As such, the birefringence can be used to determine the strength of the Rashba SOI in the region of interest in the system.

We believe that the concept of birefringent electron optics established here can lead to important consequences in experiments and applications. For example, using guiding gates [7] over graphene samples grown on Ni[111], or creating a suitable spatial pattern of gold intercalation, one could design a birefringent waveguide with two different critical angles ($\theta_{\pm} = \sin^{-1}(k_{\pm}/k)$) for the two orthogonal chiral states of the system, leading to the independent propagation of chiral states, with the corresponding spatial modulation of the spin components [31].

We thank M. Zarea and N. Sandler for useful discussions and the support of NSF CIAM/MWN and PIRE grants.

* asmar@phy.ohiou.edu

† ulloa@ohio.edu

- [1] K. W. Baldwin, L. N. Pfeiffer, J. Spector, H. L. Stormer, and K. W. West, "Aparatus comprising refractive means for electrons," US Patent 5,051,791 (1991).
- [2] K. S. Novoselov *et al.*, Science **306**, 666 (2004).
- [3] A. H. Castro Neto *et al.*, Rev. Mod. Phys. **81**, 109 (2009).
- [4] G. W. Semenoff, Phys. Rev. Lett. **53**, 2449 (1984).
- [5] M. I. Katsnelson, K. S. Novoselov and A. K. Geim, Nature Phys. **2**, 620 (2006).
- [6] F. Young and P. Kim, Nature Phys. **5**, 222 (2009).
- [7] J. R. Williams *et al.*, Nature Nanotech. **6**, 222 (2011).
- [8] V. V. Cheianov, V. Fal'ko and B. L. Altshuler, Science **315**, 1252 (2007).
- [9] V. G. Veselago, Sov. Phys. Usp. **10**, 509 (1968).
- [10] J. Cserti, A. Palyi and C. Peterfalvi, Phys. Rev. Lett. **99**, 246801 (2007).
- [11] E. W. Hill *et al.*, IEEE Trans. Magn. **42**, 2694 (2006).
- [12] S. Cho, Y.-F. Chen and M. S. Fuhrer, Appl. Phys. Lett. **91**, 123105 (2007).
- [13] W. Han *et al.*, Proc. SPIE. **8100**, 81000Q (2011).
- [14] M. H. D. Guimaraes *et al.*, Nano Lett. **12**, 3512 (2012).
- [15] W. Han *et al.*, Nano Lett. **12**, 3443 (2012).
- [16] N. Tombros *et al.*, Nature **448**, 571 (2007).
- [17] A. H. Castro Neto and F. Guinea, Phys. Rev. Lett. **103**, 026804 (2009).
- [18] K. Pi *et al.*, Phys. Rev. Lett. **104**, 187201 (2010).
- [19] C. L. Kane and E. J. Mele, Phys. Rev. Lett. **95**, 226801 (2005).
- [20] D. Huertas-Hernando, F. Guinea, and A. Brataas, Phys. Rev. B **74**, 155426 (2006); J.-S. Jeong, J. Shin, and H.-W. Lee, *ibid.* **84**, 195457 (2011).
- [21] A. Varykhalov *et al.*, Phys. Rev. Lett. **101**, 157601 (2008); D. Marchenko *et al.*, arXiv:1208.4265v1 (2012).
- [22] H. Min *et al.*, Phys. Rev. B **74**, 165310 (2006); S. Kon-schuh, M. Gmitra, and J. Fabian, Phys. Rev. B **82**, 245412 (2010).
- [23] M. V. Berry, Adv. Phys. **25**, 1 (1976).
- [24] B. Özyilmaz *et al.*, Appl. Phys. Lett. **91**, 192107 (2007).
- [25] B. Huard *et al.*, Phys. Rev. Lett. **98**, 236803 (2007).
- [26] C. Tao *et al.*, Nature Phys. **7**, 616 (2011).
- [27] K. K. Gomes *et al.*, Nature **483**, 306 (2012).
- [28] J. Martin *et al.*, Nature Phys. **4**, 144 (2008).
- [29] M. R. Connolly *et al.*, Appl. Phys. Lett. **96**, 113501 (2012).
- [30] D. S. Novikov, Phys. Rev. B **76**, 245435 (2007).
- [31] D. Bercioux *et al.*, Appl. Phys. Lett. **101**, 122405 (2012).